NANO LETTERS

Letter

pubs.acs.org/NanoLett

High Electrochemical Selectivity of Edge versus Terrace Sites in Two-Dimensional Layered MoS_2 Materials

Haotian Wang,[†] Qianfan Zhang,*[,‡] Hongbin Yao,[§] Zheng Liang,[§] Hyun-Wook Lee,[§] Po-Chun Hsu,[§] Guangyuan Zheng,[∥] and Yi Cui*[,§,⊥]

[†]Department of Applied Physics, Stanford University, Stanford, California 94305, United States

[‡]School of Materials Science and Engineering, Beihang University, Beijing 100191, People's Republic of China

[§]Department of Materials Science and Engineering and [∥]Department of Chemical Engineering, Stanford University, Stanford, California 94305, United States

[⊥]Stanford Institute for Materials and Energy Sciences, SLAC National Accelerator Laboratory, 2575 Sand Hill Road, Menlo Park, California 94025, United States

Supporting Information

ABSTRACT: Exploring the chemical reactivity of different atomic sites on crystal surface and controlling their exposures are important for catalysis and renewable energy storage. Here, we use two-dimensional layered molybdenum disulfide (MoS_2) to demonstrate the electrochemical selectivity of edge versus terrace sites for Li−S batteries and hydrogen evolution reaction (HER). Lithium sulfide (Li_2S) nanoparticles decorates along the edges of the MoS_2 nanosheet versus terrace, confirming the strong binding energies between Li_2S and the edge sites and guiding the improved electrode design for Li−S batteries. We also provided clear comparison of HER activity between edge and terrace sites of MoS_2 beyond the previous theoretical prediction and experimental proof.

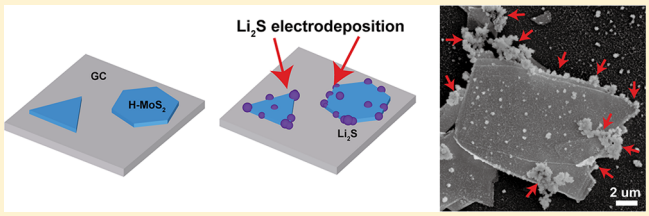

KEYWORDS: *Electrochemical selectivity, Two-dimensional materials, MoS_2, Li−S batteries, Hydrogen evolution reaction*

Understanding the effects of different atomic sites on crystal surface is critical to control chemical reactions with great importance, ranging from materials synthesis, catalysis, to energy storage.[1−8] Exposed facets, corners, steps, kinks, and edges on the surfaces of crystals have been shown to exhibit different chemical reactivity.[9−15] Two-dimensional (2D) layered crystal materials have recently attracted tremendous interests as electronic, optoelectronic, and catalytic materials.[16−19] They have strong intralayer covalent bonding and weak interlayer van der Waals force and are expected to manifest the difference of chemical reactivity between the edge sites with uncoordinated atoms and the fully coordinated terrace sites.[12,13] There exist a few examples on the different chemical reactivity of terrace and edge sites of 2D materials. The terrace and edge sites of graphite electrodes in lithium ion batteries exhibit dissimilar electrochemical reactivity during the solid electrolyte interface formation.[20] Electrodeposition of materials takes place preferentially at the line edges of graphite, resulting in the formation of nanowires.[13,21] The edge sites of molybdenum disulfide (MoS_2) show much higher electrochemical catalytic activity than the terrace counterpart in catalyzing hydrodesulfurization and hydrogen evolution.[12,22] Therefore, understanding the properties of the sites and manipulating the proper site exposure on the surface of 2D materials becomes important in materials synthesis, batteries, and catalysis.

In this work, we exploit well-defined edge-exposed (layer vertically aligned nanofilms) and terrace-exposed (horizontal nanosheets and nanocages) MoS_2 samples to demonstrate high electrochemical selectivity of edge versus terrace sites for lithium sulfide (Li_2S) electrochemical deposition in high energy Li−S batteries and electrocatalysis of hydrogen evolution reaction (HER). Recently Li−S batteries have been heavily investigated due to the low cost, high specific capacity of S (1673 mAh/g), and high theoretical specific energy (2600 Wh/kg),[23,24] which are attractive for portable electronics and electrical transportations.[25] However, the polysulfide dissolution during battery charge/discharge has been a major challenge causing capacity decay.[25,26] Many approaches have been developed to address this challenge including (1) physical confinement of polysulfide with porous nanostructures, polymers, rationally designed hollow nanoparticles and yolk−shell structures,[23,27−31] (2) increasing chemical interaction with polysulfide using polar polymers and inorganics,[32,33] (3) changing electrolyte to reduce polysulfide solubility,[34] and (4) dispersing S into microporous structures to avoid polysulfide formation.[35] In all these studies, appreciable amount (10−15%) of polysulfide dissolution still takes place, causing the capacity

Received: September 29, 2014
Revised: November 3, 2014

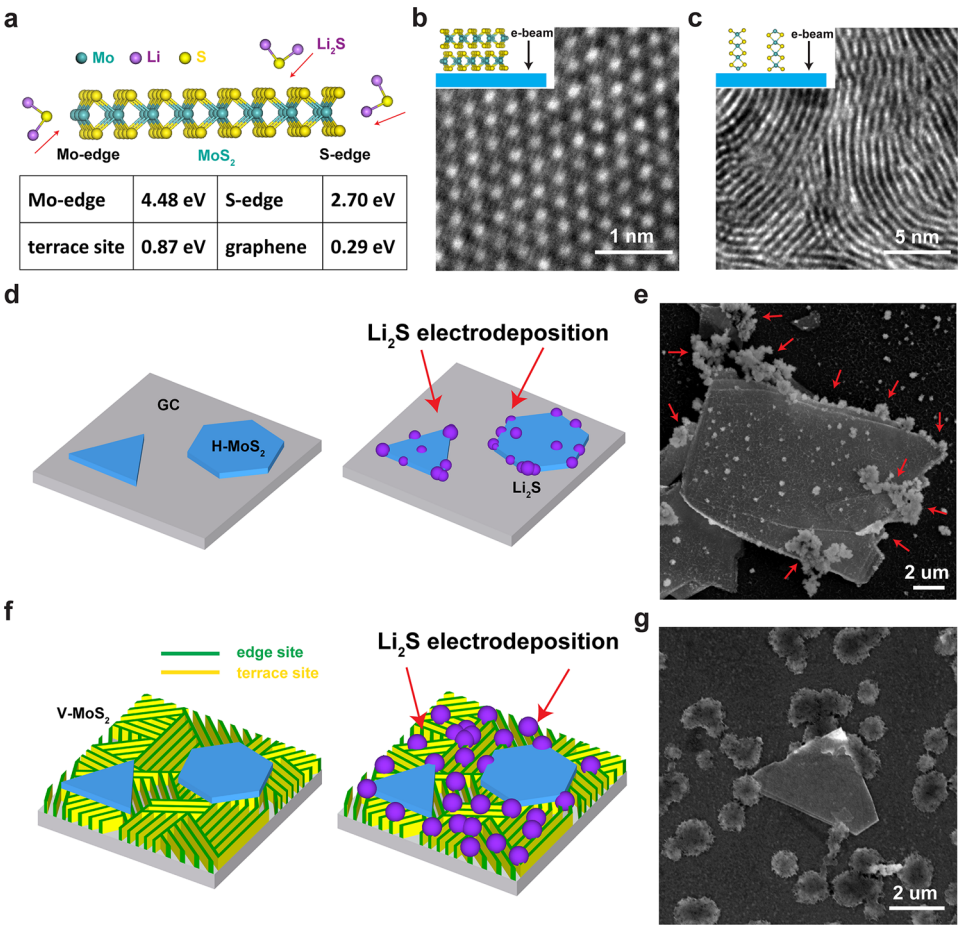

Mo-edge	4.48 eV	S-edge	2.70 eV
terrace site	0.87 eV	graphene	0.29 eV

Figure 1. Simulations, characterizations, and schematics of Li_2S electrochemical deposition onto different sites of MoS_2. (a) Schematic of the interaction between Li_2S molecules and different MoS_2 atomic sites. The calculated binding energies are summarized. (b,c) TEM images of exfoliated H-MoS_2 single layer with hexagonal lattice and V-MoS_2 nanofilm with edge sites exposed. The inset shows the e-beam direction. (d) Schematic of H-MoS_2 nanosheets on GC substrate with Li_2S electrodepostion. Li_2S NPs tend to be deposited onto the MoS_2 edge sites. (e) SEM image of H-MoS_2 nanosheet with Li_2S NPs decorated along the edges as indicated by the red arrows. Only a few smaller NPs are randomly distributed on the terrace surface and GC substrate. (f) Schematic of H-MoS_2 nanosheet on edge-terminated V-MoS_2 nanofilm. Li_2S NPs are attracted by the MoS_2 edges on the substrate. (g) SEM image of H-MoS_2 on V-MoS_2 nanofilm without obvious edge effects as panel e due to the competition from the edge sites on the substrate.

decay. Therefore, controlling spatially the electrochemical deposition of soluble polysulfides is important as shown recently in selective deposition of S species on conducting oxide surface instead of carbon.[33] In addition to Li−S batteries, Li metal polysulfide semiflow batteries as an attractive concept for grid-scale energy storage also calls for the controlled deposition of polysulfides.[36]

We recently demonstrated that 2D transition metal disulfides are effective encapsulation materials for improved Li_2S cathodes due to the strong interactions with Li_2S;[37] however, the site-dependent binding energies with S species are still unclear. Understanding polysulfide binding with different crystal sites is critical for controlled polysulfide deposition. We propose that 2D layered materials afford well-defined model system to understand site-dependent deposition due the drastic difference of edge and terrace sites and are potentially practical solutions.

Results and Discussions. We first demonstrate the electrochemical site selectivity by the ab initio simulation. The calculated binding energy between Li_2S molecule and the MoS_2 terrace and edge sites are summarized in Figure 1a and Supporting Information Figure S1 (Supporting Information Materials and Methods). The binding energy with MoS_2 terrace site is ∼0.87 eV, slightly higher than the case of graphene (0.29 eV).[32] The MoS_2 edge sites, including the Mo-edge and S-edge, have unsaturated dangling bonds that help to interact with Li_2S much more strongly than the terrace counterpart. The binding energies for the Mo-edge and S-edge are 4.48 and 2.70 eV, respectively. Under certain conditions, the Mo-edge can have 50 or 100% S coverage.[9] Simulations on those S covered Mo-edge site still exhibits large binding energies with Li_2S (Supporting Information Figure S1). These simulation results suggest a large selectivity of edge versus terrace sites.

In order to demonstrate experimentally the site selectivity, we have generated thin sheets of MoS_2 lying horizontally (H-MoS_2) on a flat conducting glassy carbon (GC) substrate by mechanical exfoliation.[16,38] As shown in the scanning electron microscopy (SEM) images in Supporting Information Figure S2, they typically exhibit irregular shapes with the lateral size distribution ranging from 1 to over 10 μm. These nanosheets are typically ∼20 nm thick as measured by atomic force microscopy (AFM) in Supporting Information Figure S3. High-resolution transmission electron microscopy (TEM) image in Figure 1b shows the hexagonal lattice of the as-exfoliated MoS_2 with the projection of the electron beam on the terrace surface

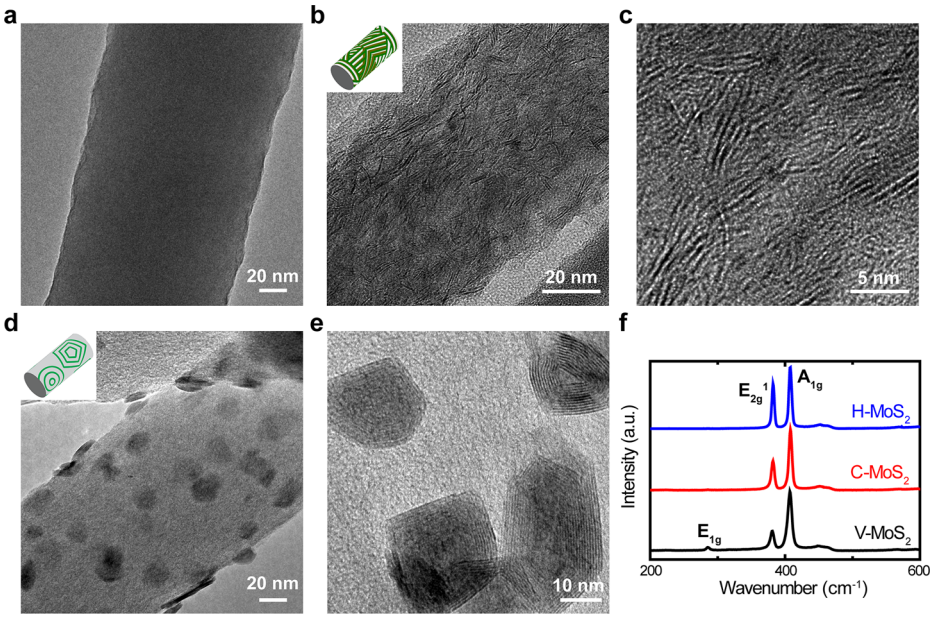

Figure 2. TEM images and Raman spectra of MoS_2 with different atomic sites exposed on CNF. (a) TEM image of a typical CNF. The diameter ranges from 100 to 200 nm. (b,c) TEM images of V-MoS_2 on CNF with edge sites exposed. The CNF surface is uniformly covered with MoS_2 edges. The inset shows the schematic of the MoS_2 structure on the CNF. (d,e) TEM images of C-MoS_2 NPs on CNF with only terrace sites exposed. MoS_2 tends to hide the exposed edge sites by forming buckyball like structure layer by layer. (f) Raman spectra of different MoS_2 structures. The integrated intensity ratio of E_{2g}^1 to A_{1g} offers rich information about the orientation of the MoS_2 molecular layers.

of the layer. A pouch battery cell, with the H-MoS_2 on GC as cathode, Li metal as anode, and 10 ul of 0.5 M Li_2S_8 polysulfide solution (based on S) as catholyte, was used to perform the electrochemical deposition with current density of 2.5 $\mu A/cm^2$ (Supporting Information Materials and Methods). As illustrated in the schematic of Figure 1d, we expect that Li_2S would tend to be deposited at edge sites due to the high binding energies of Li_2S species there. The SEM image in Figure 1e shows that the deposited Li_2S NPs are mostly distributed at the edges of the nanosheet highlighted by the arrows. On top of the nanosheet there are visible steps with additional exposed edge sites, which also bind a large number of Li_2S particles. Compared with the MoS_2 edge sites, there are only a few Li_2S NPs with much smaller sizes distributed on the terrace surface of the nanosheet and the GC substrate. We note that the NPs are still decorated along the edges during charging the battery for S deposition as shown in Supporting Information Figure S4a, suggesting the same electrochemical selectivity of the edges for S deposition.[33] However, this selectivity would be lost if we use mild oxidation to pretreat MoS_2 (Supporting Information Figure S4b, Materials and Methods), which would change the surface functional groups on both edge and a part of terrace sites to O or OH groups.[39] No obvious edge effects observed in Supporting Information Figure S4b again confirms that the high electrochemical selectivity results from the interaction of Li_2S and the fresh edge sites and, more importantly, rules out any possible physical geometric influences on the Li_2S deposition.

To further show the edge selectivity, we use an edge-terminated surface to study the electrodeposition. Recently, we developed a method of the rapid sulfurization reaction to convert Mo thin film (5 nm) into layer vertically aligned MoS_2 (V-MoS_2) thin film (20 nm) on the GC substrate (Supporting Information Materials and Methods).[40] As shown in the TEM image in Figure 1c the MoS_2 layers are parallel to the electron beam, or perpendicular to the substrate, with nearly 100% edge sites exposed on the surface. We used mechanical exfoliation to transfer some MoS_2 nanosheets onto the V-MoS_2 thin film and created a sample with mostly edge sites and a few terrace sites. We expect that the distribution of Li_2S NPs after electrodeposition will change significantly when the MoS_2 edge-terminated surface substitutes for the carbon surface as illustrated in Figure 1f. The ability of the H-MoS_2 edges to attract S species for deposition is reduced to a considerable extent due to the rising competition from the V-MoS_2 edge sites. Li_2S NPs tend to be randomly distributed on the whole surface area except for the terrace surface of the H-MoS_2. In Figure 1g, there are Li_2S particles sitting along the edges of the nanosheet; however, even more particles are distributed around the nanosheet, showing no distinct H-MoS_2 edge effects. No Li_2S NPs are observed on the terrace surface of the H-MoS_2 except for the corners. Notice that the sizes and morphologies of the Li_2S NPs are different from those in Figure 1e, possibly due to the varied surface chemistry, which definitely influences the nucleation process.[41] A comparison of the selectivity between MoS_2 edge sites and carbon is by the distribution of electrodeposited Li_2S NPs on these two patterned surfaces (Supporting Information Figure S5). The Li_2S NPs are concentrated on the MoS_2 edge-terminated instead of the GC surface, again confirming the strong electrochemical selectivity of MoS_2 edge sites.

With all the above simulation and experimental results, we can conclude that MoS_2 edge sites have much higher electrochemical selectivity and activity than its terrace surface, which provides important guidance to the battery electrode materials design. Here we use this design principle of maximizing edge site exposure to synthesize three-dimensional electrodes for studying the Li−S battery cell performance. A free-standing, high surface area and low weight-conducting carbon nanofiber (CNF) matrix (Supporting Information Figure S6) is obtained by electrospinning the nanofibers of polyacrylonitrile (PAN) and polypyrrolidone (PVP) followed

dx.doi.org/10.1021/nl503730c | Nano Lett. XXXX, XXX, XXX−XXX

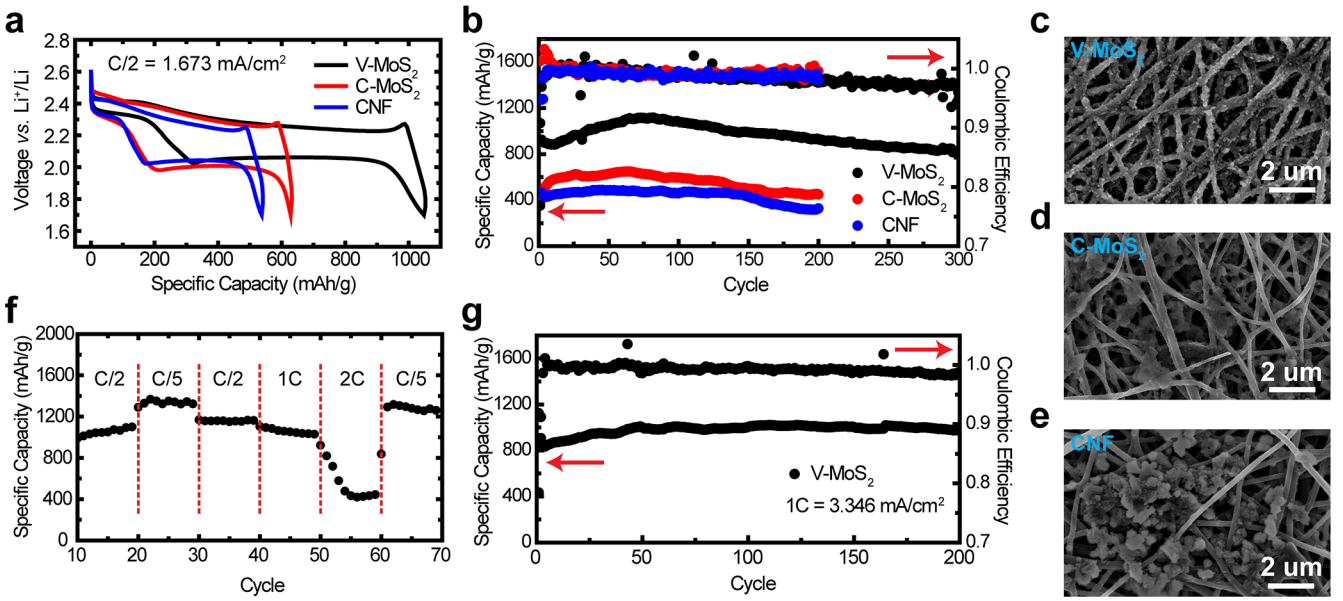

Figure 3. Li–S battery testing and SEM images of different electrodes. (a) Discharge/charge voltage profiles (C/2) at 50th cycle of the V-MoS_2–CNF, C-MoS_2–CNF, and bare CNF electrodes. The specific capacity of V-MoS_2–CNF is over 1000 mAh/g, nearly twice of the C-MoS_2–CNF and bare CNF. (b) Cycling performance (C/2) of the V-MoS_2–CNF, C-MoS_2–CNF, and bare CNF electrodes. V-MoS_2–CNF maintains over 800 mAh/g capacity for over 300 cycles, showing good cycling stability. (c–e) SEM images of Li_2S deposition after 50 cycles onto the V-MoS_2–CNF, C-MoS_2–CNF, and bare CNF electrodes, respectively. On V-MoS_2 surface Li_2S is uniformly distributed without any aggregations. On the contrary, the C-MoS_2–CNF and bare CNF without strong selectivity suffer from large aggregations of Li_2S. (f) Rate capability of V-MoS_2–CNF electrode. (g) High rate cycling (1C = 3.345 mA/cm^2) performance of V-MoS_2–CNF electrode. Over 1000 mAh/g specific capacity is achieved for 200 cycles without degradation.

by a simple carbonization process (Supporting Information Materials and Methods).[42] The TEM image in Figure 2a shows a typical CNF with the diameter of 100 to 200 nm. To coat the carbon surface with MoS_2 edges, we employed the simple dip-coating of ammonium molybdate solution method for MoO_3 NPs synthesis, followed by the rapid sulfurization process under 600 °C to become MoS_2 (Supporting Information Materials and Methods).[43] The TEM images in Figure 2b,c as well as the inset schematic clearly reveal that the MoS_2 layers are vertically standing on the CNF with edges exposed. The blurred areas without observable edges in the images may be due to the tilted layers on the curved surface of the CNF.[44] The edge and terrace site exposure can be easily manipulated by adjusting the sulfurization temperature and time. For example, we can also reduce the edge site exposure to minimum by forming cage-like MoS_2 nanoparticles (C-MoS_2) with self-closed layers, also known as inorganic fullerene-like MoS_2 NPs (Figure 2d,e),[45,46] simply by increasing the reaction temperature to 800 °C and the growth time to 5 h. The C-MoS_2 exposes terrace sites instead of the edge sites. The C-MoS_2 is considered to be thermodynamically more stable than the V-MoS_2,[40] which explains why the C-MoS_2 dominates under the high-temperature, long growth time condition.[46] The comparison of Raman spectra among the three different MoS_2 structures (H-MoS_2, V-MoS_2, C-MoS_2) in Figure 2f is very intriguing and offers rich information. The H-MoS_2 nanosheet exhibits E_{2g}^1 and A_{1g} vibration modes with similar integrated intensities ($E_{2g}^1/A_{1g} \approx$ 1:1.4), consistent with previous studies.[47] V-MoS_2 has a completely different intensity ratio of E_{2g}^1 to A_{1g} ($\approx$ 1:3) where the A_{1g} mode with the out of plane vibration direction is favored by the layer vertically standing structure.[40,48] The intensity ratio of C-MoS_2 ($\approx$ 1:2) positions well within the range of the two limiting conditions due to the curved molecular layers.[40]

Li–S batteries were assembled to compare the following three types of cathodes: (1) the V-MoS_2 edge-terminated CNF (V-MoS_2–CNF) electrode, (2) the C-MoS_2–CNF, and (3) bare CNF (Supporting Information Materials and Methods). The electrodes are free of binder and carbon additives. Polysulfide solutions (Li_2S_8) equivalent to 2 mg/cm^2 of S were added as the starting material (Supporting Information Materials and Methods). The batteries were discharged to 1.7 V and then charged back to 2.6 V at a C/2 rate of 1.673 mA/cm^2. The V-MoS_2–CNF electrode delivers reversible specific capacity value of 1052 mAh/g at the 50th cycle, while the C-MoS_2–CNF and bare CNF substrates obtain only 628 and 536 mAh/g respectively, only half of the V-MoS_2–CNF capacity as shown in Figure 3a. The significant difference between the capacities can be explained by the SEM images of the Li_2S deposition on those electrodes after running 50 cycles in Figure 3c–e. The V-MoS_2–CNF in Figure 3c with high electrochemical selectivity shows uniformly distributed Li_2S NPs with diameters below 200 nm and no large particles. However, the C-MoS_2–CNF electrode without the edge sites exposed shows the uneven distribution and large Li_2S particles (Figure 3d). Large size particles on the fibers suggest that there are not enough active sites for Li_2S to be deposited, further confirming the much stronger electrochemical selectivity of the edges over the terrace surface. The bare CNF in Figure 3e has even weaker bonding with the Li_2S NPs, resulting in a great number of large particles in micrometers. SEM images with different magnifications are shown in Supporting Information Figure S7. Those aggregated particles suffer weak electrical contact with the substrate, which explains the lower capacity than the V-MoS_2–CNF electrode. The electrochemical selectivity of the edge sites

dx.doi.org/10.1021/nl503730c | Nano Lett. XXXX, XXX, XXX–XXX

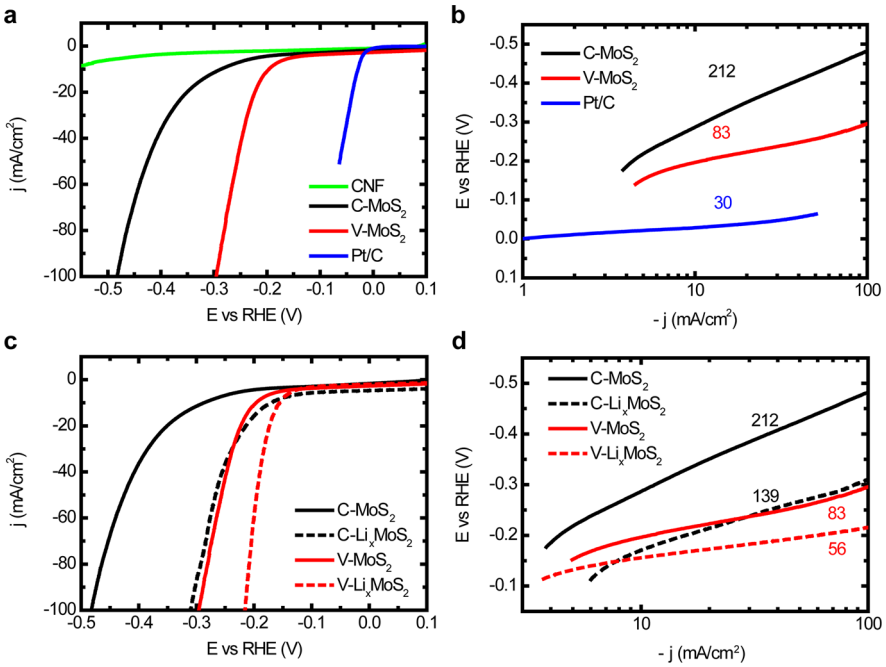

Figure 4. Electrochemical selectivity of the edge and terrace sites in catalyzing HER. (a) Polarization curves of the V-MoS_2−CNF, C-MoS_2−CNF, and bare CNF on carbon fiber paper electrodes. The 100 mA/cm^2 cathodic current is achieved by V-MoS_2 before 300 mV overpotential, suggesting the high HER catalytic activity of the edge sites. Inferior performance is shown in C-MoS_2 sample that indicates the weaker selectivity of the terrace sites. (b) Tafel plots of the V-MoS_2−CNF and C-MoS_2−CNF on carbon fiber paper substrate. V-MoS_2−CNF shows an 83 mV/decade Tafel slope while C-MoS_2−CNF suffers from sluggish reaction process with a large Tafel slope of 212 mV/decade. (c) Polarization curves of the V-MoS_2−CNF and C-MoS_2−CNF catalysts before and after Li electrochemical intercalation. The electrochemical tuning method can effectively improve both catalysts. The best performance is achieved by V-MoS_2−CNF after Li tuning, which reaches 100 mA/cm^2 at only 216 mV overpotential. (d) Tafel plots of the V-MoS_2−CNF and C-MoS_2−CNF catalysts before and after Li electrochemical intercalation. The Tafel slopes of the V-MoS_2−CNF and C-MoS_2−CNF are improved to 139 and 56 mV/decade after the tuning process.

plays an important role in controlling the Li_2S spatial distribution and as a result improving the performance of the battery.

Cycling stability of the V-MoS_2−CNF electrode was tested at C/2 for over 300 cycles in Figure 3b. The first discharge capacity is 1068 mAh/g with some decay until the 10th cycle followed by a slow activation process to reach 1110 mAh/g at the 65th cycle. The initial decay is likely due to the reaction of polysulfides with Li metal. At the 300th cycle over 800 mAh/g (∼75% of the first cycle), specific capacity is retained with an average capacity decay of only 0.08% per cycle. Over the cycles, the discharge capacity of V-MoS_2 is nearly twice of the C-MoS_2−CNF and bare CNF. Good rate capability of the V-MoS_2−CNF electrode is illustrated in Figure 3f with reversible specific capacities of 1339, 1152, and 1066 mAh/g at C/5, C/2, and 1C respectively. The capacity drops dramatically at 2C rate, which we assume is due to the diffusion limit of polysulfide species in the electrolyte.[49] We tested our V-MoS_2−CNF Li−S battery at 1C rate with impressive charge/discharge current density of 3.346 mA/cm^2 for 200 cycles, achieving over 1000 mAh/g without any capacity decrease. The outstanding performance of the high rate testing benefits from the facile electrochemical deposition of S species on the V-MoS_2 edge-terminated surface.

The electrochemical selectivity of 2D material edge sites also plays a critical role in electrocatalysis.[12,22] For example, under the hydrogen evolution condition, the specific atomic structure of MoS_2 edge sites provides a proper bonding (not too strong and not too weak) with H, which facilitates both the discharge step and the H_2 releasing process.[12] In the past, measurements on horizonatal nanoplates of MoS_2 were conducted to show that HER activity is linearly scaled with edge lengths,[22] as an evidence of active edge sites. Recent simulation results also show a large free energy of H bonding on terrace sites compared with the edge sites, confirming that the terrace sites are not active for HER.[50] However, there have not been any studies to compare the edge-only and terrace-only samples experimentally. Here our V-MoS_2−CNF and C-MoS_2−CNF electrodes afford such a possibility. The V-MoS_2−CNF matrix was first broken down into small pieces by ball milling, and then uniformly drop casted onto carbon fiber paper substrate with binders and carbon additives for efficient electron transport and bubble releasing (Supporting Information Materials and Methods). The mass loading of MoS_2 is ∼0.25 mg/cm^2. A standard three-electrode setup was used for performing electrochemical characterizations in 0.5 M H_2SO_4 solution (Supporting Information Materials and Methods). The performances of the catalysts are *iR*-corrected. In Figure 4a, a large cathodic current of 100 mA/cm^2 is obtained by V-MoS_2−CNF at less than 300 mV overpotential versus reversible hydrogen electrode (RHE), indicating a high electrochemical catalytic activity of the MoS_2 edge sites.[22,51−53] As a sharp contrast, the C-MoS_2−CNF without the edge exposure exhibits much lower activity in catalyzing HER. The Tafel plots in Figure 4b suggest that the kinetics of the electrochemical hydrogen evolution on MoS_2 edge sites is much faster than the terrace sites. Two possible reasons are responsible for the poor performance of the C-MoS_2. The main reason is much less exposure of the active edge sites; the other is that the layer orientation may result in lower conductivity compared with the

layer vertically aligned structure.[40] We also tested the electrochemical double layer capacity of C-MoS_2−CNF and V-MoS_2−CNF as a direct comparison of their active surface areas. The capacity of V-MoS_2−CNF is 16.0 mF, significantly higher than that of C-MoS_2−CNF (1.3 mF). This large difference in capacity confirms that the HER active surface area of V-MoS_2−CNF is larger than C-MoS_2−CNF (Supporting Information Figure S8). The stability of the V-MoS_2−CNF catalyst was tested by applying a constant voltage to achieve ∼10 mA/cm^2 cathodic current for over 2 h (Supporting Information Figure S9). The negligible decay of the current suggests that catalyst is stable under the evolution condition.[43] In addition, the morphology of C-MoS_2 after constant HER current operation is slightly changed with the cage partially opened as indicated in Supporting Information Figure S10. The HER performance of V-MoS_2−CNF could be further optimized by the Li electrochemical tuning method developed in our previous studies (Supporting Information Materials and Methods).[43,48] Here both V-MoS_2−CNF and C-MoS_2−CNF are improved by much as shown in Figure 4c,d. The intercalated Li helps to dramatically change the electronic structure of MoS_2 from 2H to 1T, creating new HER active sites, and at the same time expanding or exfoliating the layers for larger surface areas.[43,48,54,55] In Supporting Information Figure S11a, it is difficult to tell whether the layers of V-MoS_2 on CNF are expanded or not after Li intercalation due to the highly curved surface of the fibers (on a flat substrate the layer spacing is expanded by ∼10%);[48] however, the C-MoS_2 is broken into a noncontinuous shape to open up some edge sites as shown in Supporting Information Figure S11b. The selectivity in catalyzing HER further reveals the importance of the 2D material edge sites in catalysis as well as other important applications.

Conclusion. This work illustrates the great importance of understanding the site-dependent chemical reactivity of 2D materials. The demonstration of electrochemical selectivity of edge versus terrace sites provides a clear guidance of 2D MoS_2 design for improved batteries and catalysis, which also opens up opportunities to design and engineer the big family of 2D materials for extended applications.

■ ASSOCIATED CONTENT

Supporting Information

Materials and Methods, Figures S1 to S11 are included. This material is available free of charge via the Internet at http://pubs.acs.org.

■ AUTHOR INFORMATION

Corresponding Authors

*E-mail: yicui@stanford.edu (Y.C.).
*E-mail: qianfan@buaa.edu.cn (Q.Z.).

Author Contributions

H.W. and Y.C. conceived the experiments. H.W., H.Y., and Z.L. synthesized and prepared the materials. H.W., H−W.L., P−C.H., and G.Z. performed characterizations. H.W., H.Y., and Z.L. carried out electrochemical measurements and analyses. Q.Z performed ab initio simulations. All authors contributed to scientific planning and discussions.

Notes

The authors declare no competing financial interest.

■ ACKNOWLEDGMENTS

We acknowledge support by the Department of Energy, Office of Basic Energy Sciences, Materials Sciences and Engineering Division, under contract DE-AC02-76-SFO0515.

■ REFERENCES

(1) Stamenkovic, V. R.; Fowler, B.; Mun, B. S.; Wang, G.; Ross, P. N.; Lucas, C. A.; Marković, N. M. *Science* **2007**, *315* (5811), 493−497.
(2) Hansen, T. W.; Wagner, J. B.; Hansen, P. L.; Dahl, S.; Topsøe, H.; Jacobsen, C. J. H. *Science* **2001**, *294* (5546), 1508−1510.
(3) Hansen, P. L.; Wagner, J. B.; Helveg, S.; Rostrup-Nielsen, J. R.; Clausen, B. S.; Topsøe, H. *Science* **2002**, *295* (5562), 2053−2055.
(4) Over, H.; Kim, Y. D.; Seitsonen, A. P.; Wendt, S.; Lundgren, E.; Schmid, M.; Varga, P.; Morgante, A.; Ertl, G. *Science* **2000**, *287* (5457), 1474−1476.
(5) Sun, Y.; Xia, Y. *Science* **2002**, *298* (5601), 2176−2179.
(6) Peng, X.; Manna, L.; Yang, W.; Wickham, J.; Scher, E.; Kadavanich, A.; Alivisatos, A. P. *Nature* **2000**, *404* (6773), 59−61.
(7) Lim, B.; Jiang, M.; Camargo, P. H. C.; Cho, E. C.; Tao, J.; Lu, X.; Zhu, Y.; Xia, Y. *Science* **2009**, *324* (5932), 1302−1305.
(8) Chen, C.; Kang, Y.; Huo, Z.; Zhu, Z.; Huang, W.; Xin, H. L.; Snyder, J. D.; Li, D.; Herron, J. A.; Mavrikakis, M.; Chi, M.; More, K. L.; Li, Y.; Markovic, N. M.; Somorjai, G. A.; Yang, P.; Stamenkovic, V. R. *Science* **2014**, *343* (6177), 1339−1343.
(9) Lauritsen, J. V.; Kibsgaard, J.; Helveg, S.; Topsoe, H.; Clausen, B. S.; Laegsgaard, E.; Besenbacher, F. *Nat. Nanotechnol.* **2007**, *2* (1), 53−58.
(10) Manna, L.; Milliron, D. J.; Meisel, A.; Scher, E. C.; Alivisatos, A. P. *Nat. Mater.* **2003**, *2* (6), 382−385.
(11) Lantz, M. A.; Hug, H. J.; Hoffmann, R.; van Schendel, P. J. A.; Kappenberger, P.; Martin, S.; Baratoff, A.; Güntherodt, H.-J. *Science* **2001**, *291* (5513), 2580−2583.
(12) Hinnemann, B.; Moses, P. G.; Bonde, J.; Jørgensen, K. P.; Nielsen, J. H.; Horch, S.; Chorkendorff, I.; Nørskov, J. K. *J. Am. Chem. Soc.* **2005**, *127* (15), 5308−5309.
(13) Zach, M. P.; Ng, K. H.; Penner, R. M. *Science* **2000**, *290* (5499), 2120−2123.
(14) Tian, N.; Zhou, Z.-Y.; Sun, S.-G.; Ding, Y.; Wang, Z. L. *Science* **2007**, *316* (5825), 732−735.
(15) Zambelli, T.; Wintterlin, J.; Trost, J.; Ertl, G. *Science* **1996**, *273* (5282), 1688−1690.
(16) Novoselov, K. S.; Geim, A. K.; Morozov, S. V.; Jiang, D.; Zhang, Y.; Dubonos, S. V.; Grigorieva, I. V.; Firsov, A. A. *Science* **2004**, *306* (5696), 666−669.
(17) Geim, A. K.; Novoselov, K. S. *Nat. Mater.* **2007**, *6* (3), 183−191.
(18) Butler, S. Z.; Hollen, S. M.; Cao, L.; Cui, Y.; Gupta, J. A.; Gutiérrez, H. R.; Heinz, T. F.; Hong, S. S.; Huang, J.; Ismach, A. F.; Johnston-Halperin, E.; Kuno, M.; Plashnitsa, V. V.; Robinson, R. D.; Ruoff, R. S.; Salahuddin, S.; Shan, J.; Shi, L.; Spencer, M. G.; Terrones, M.; Windl, W.; Goldberger, J. E. *ACS Nano* **2013**, *7* (4), 2898−2926.
(19) Chhowalla, M.; Shin, H. S.; Eda, G.; Li, L.-J.; Loh, K. P.; Zhang, H. *Nat. Chem.* **2013**, *5* (4), 263−275.
(20) Zhang, S.; Ding, M. S.; Xu, K.; Allen, J.; Jow, T. R. *Electrochem. Solid-State Lett.* **2001**, *4* (12), A206−A208.
(21) Walter, E. C.; Zach, M. P.; Favier, F.; Murray, B. J.; Inazu, K.; Hemminger, J. C.; Penner, R. M. *ChemPhysChem* **2003**, *4* (2), 131−138.
(22) Jaramillo, T. F.; Jørgensen, K. P.; Bonde, J.; Nielsen, J. H.; Horch, S.; Chorkendorff, I. *Science* **2007**, *317* (5834), 100−102.
(23) Ji, X.; Lee, K. T.; Nazar, L. F. *Nat. Mater.* **2009**, *8* (6), 500−506.
(24) Bruce, P. G.; Freunberger, S. A.; Hardwick, L. J.; Tarascon, J.-M. *Nat. Mater.* **2012**, *11* (1), 19−29.
(25) Yang, Y.; Zheng, G.; Cui, Y. *Chem. Soc. Rev.* **2013**, *42* (7), 3018−3032.
(26) Ji, X.; Nazar, L. F. *J. Mater. Chem.* **2010**, *20* (44), 9821−9826.
(27) Zheng, G.; Yang, Y.; Cha, J. J.; Hong, S. S.; Cui, Y. *Nano Lett.* **2011**, *11* (10), 4462−4467.

(28) Jayaprakash, N.; Shen, J.; Moganty, S. S.; Corona, A.; Archer, L. A. *Angew. Chem.* **2011**, *123* (26), 6026−6030.
(29) Xiao, L.; Cao, Y.; Xiao, J.; Schwenzer, B.; Engelhard, M. H.; Saraf, L. V.; Nie, Z.; Exarhos, G. J.; Liu, J. *Adv. Mater.* **2012**, *24* (9), 1176−1181.
(30) Seh, Z. W.; Li, W.; Cha, J. J.; Zheng, G.; Yang, Y.; McDowell, M. T.; Hsu, P.-C.; Cui, Y. *Nat. Commun.* **2013**, *4*, 1331.
(31) Moon, S.; Jung, Y. H.; Jung, W. K.; Jung, D. S.; Choi, J. W.; Kim, D. K. *Adv. Mater.* **2013**, *25* (45), 6547−6553.
(32) Zheng, G.; Zhang, Q.; Cha, J. J.; Yang, Y.; Li, W.; Seh, Z. W.; Cui, Y. *Nano Lett.* **2013**, *13* (3), 1265−1270.
(33) Yao, H.; Zheng, G.; Hsu, P.-C.; Kong, D.; Cha, J. J.; Li, W.; Seh, Z. W.; McDowell, M. T.; Yan, K.; Liang, Z.; Narasimhan, V. K.; Cui, Y. *Nat. Commun.* **2014**, *5*, 5280.
(34) Suo, L.; Hu, Y.-S.; Li, H.; Armand, M.; Chen, L. *Nat. Commun.* **2013**, *4*, 1481.
(35) Xin, S.; Gu, L.; Zhao, N.-H.; Yin, Y.-X.; Zhou, L.-J.; Guo, Y.-G.; Wan, L.-J. *J. Am. Chem. Soc.* **2012**, *134* (45), 18510−18513.
(36) Yang, Y.; Zheng, G.; Cui, Y. *Energy Environ. Sci.* **2013**, *6* (5), 1552−1558.
(37) Seh, Z. W.; Yu, J. H.; Li, W.; Hsu, P.-C.; Wang, H.; Sun, Y.; Yao, H.; Zhang, Q.; Cui, Y. *Nat. Commun.* **2014**, *5*, 5017.
(38) Radisavljevic, B.; Radenovic, A.; Brivio, J.; Giacometti, V.; Kis, A. *Nat. Nanotechnol.* **2011**, *6* (3), 147−150.
(39) Voiry, D.; Salehi, M.; Silva, R.; Fujita, T.; Chen, M.; Asefa, T.; Shenoy, V. B.; Eda, G.; Chhowalla, M. *Nano Lett.* **2013**, *13* (12), 6222−6227.
(40) Kong, D.; Wang, H.; Cha, J. J.; Pasta, M.; Koski, K. J.; Yao, J.; Cui, Y. *Nano Lett.* **2013**, *13* (3), 1341−1347.
(41) Tian, M.; Wang, J.; Kurtz, J.; Mallouk, T. E.; Chan, M. H. W. *Nano Lett.* **2003**, *3* (7), 919−923.
(42) Li, D.; Xia, Y. *Adv. Mater.* **2004**, *16* (14), 1151−1170.
(43) Wang, H.; Lu, Z.; Kong, D.; Sun, J.; Hymel, T. M.; Cui, Y. *ACS Nano* **2014**, *8* (5), 4940−4947.
(44) Wang, H.; Kong, D.; Johanes, P.; Cha, J. J.; Zheng, G.; Yan, K.; Liu, N.; Cui, Y. *Nano Lett.* **2013**, *13* (7), 3426−3433.
(45) Tenne, R.; Margulis, L.; Genut, M.; Hodes, G. *Nature* **1992**, *360* (6403), 444−446.
(46) Feldman, Y.; Wasserman, E.; Srolovitz, D. J.; Tenne, R. *Science* **1995**, *267* (5195), 222−225.
(47) Lee, C.; Yan, H.; Brus, L. E.; Heinz, T. F.; Hone, J.; Ryu, S. *ACS Nano* **2010**, *4* (5), 2695−2700.
(48) Wang, H.; Lu, Z.; Xu, S.; Kong, D.; Cha, J. J.; Zheng, G.; Hsu, P.-C.; Yan, K.; Bradshaw, D.; Prinz, F. B.; Cui, Y. *Proc. Natl. Acad. Sci. U.S.A.* **2013**, *110* (49), 19701−19706.
(49) Shin, E. S.; Kim, K.; Oh, S. H.; Cho, W. I. *Chem. Commun.* **2013**, *49* (20), 2004−2006.
(50) Tsai, C.; Chan, K.; Abild-Pedersen, F.; Norskov, J. K. *Phys. Chem. Chem. Phys.* **2014**, *16* (26), 13156−13164.
(51) Kibsgaard, J.; Chen, Z.; Reinecke, B. N.; Jaramillo, T. F. *Nat. Mater.* **2012**, *11* (11), 963−969.
(52) Chen, Z.; Cummins, D.; Reinecke, B. N.; Clark, E.; Sunkara, M. K.; Jaramillo, T. F. *Nano Lett.* **2011**, *11* (10), 4168−4175.
(53) Li, Y.; Wang, H.; Xie, L.; Liang, Y.; Hong, G.; Dai, H. *J. Am. Chem. Soc.* **2011**, *133* (19), 7296−7299.
(54) Lukowski, M. A.; Daniel, A. S.; Meng, F.; Forticaux, A.; Li, L.; Jin, S. *J. Am. Chem. Soc.* **2013**, *135* (28), 10274−10277.
(55) Voiry, D.; Yamaguchi, H.; Li, J.; Silva, R.; Alves, D. C. B.; Fujita, T.; Chen, M.; Asefa, T.; Shenoy, V. B.; Eda, G.; Chhowalla, M. *Nat. Mater.* **2013**, *12* (9), 850−855.